Synthesis, Evaluation, and Metabolism of Novel [6]-Shogaol Derivatives as Potent Nrf2 Activators

Yingdong Zhu, Pei Wang, Yantao Zhao, Chun Yang, Anderson Clark, TinChung Leung, Xiaoxin Chen, Shengmin Sang

www.elsevier.com

PII: S0891-5849(16)30005-3
DOI: http://dx.doi.org/10.1016/j.freeradbiomed.2016.03.026
Reference: FRB12803

To appear in: *Free Radical Biology and Medicine*

Received date: 12 January 2016
Revised date: 4 March 2016
Accepted date: 24 March 2016

Cite this article as: Yingdong Zhu, Pei Wang, Yantao Zhao, Chun Yang, Anderson Clark, TinChung Leung, Xiaoxin Chen and Shengmin Sang, Synthesis, Evaluation, and Metabolism of Novel [6]-Shogaol Derivatives as Potent Nrf2 Activators, *Free Radical Biology and Medicine,* http://dx.doi.org/10.1016/j.freeradbiomed.2016.03.026

Synthesis, Evaluation, and Metabolism of Novel [6]-Shogaol Derivatives as Potent Nrf2 Activators

Yingdong Zhu [a], Pei Wang [a], Yantao Zhao [a], Chun Yang [a, b], Anderson Clark [c], TinChung Leung [c], Xiaoxin Chen [d], and Shengmin Sang [1,*]

[a] Laboratory for Functional Foods and Human Health, Center for Excellence in Post-Harvest Technologies, North Carolina Agricultural and Technical State University, North Carolina Research Campus, 500 Laureate Way, Kannapolis, NC 28081, USA

[b] Department of Colorectal Surgery, General Hospital of Ningxia Medical University, Yinchuan 750004, P.R. China

[c] Nutrition Research Program, Julius L. Chambers Biomedical/Biotechnology Research Institute, North Carolina Central University, North Carolina Research Campus, 500 Laureate Way, Kannapolis, NC 28081, USA

[d] Cancer Research Program, Julius L. Chambers Biomedical/Biotechnology Research Institute, North Carolina Center University, 700 George Street, Durham, NC 27707, USA

* Corresponding author. Fax: 704-250-5709, E-mail: ssang@ncat.edu or shengminsang@yahoo.com (S. Sang)

Abbreviations: ARE, antioxidant response element; br, broad; 6G, [6]-gingerol; GFP, green fluorescent protein; gstp 1, glutathione *S*-transferase pi 1; hpf, hours postfertilization; Keap1, Kelch-like ECH-associated protein 1; LC/MS, liquid chromatography-mass spectrometry; Nrf2, nuclear factor erythroid 2 p45-related factor 2; 6S, [6]-shogaol; SFN, sulforaphane; TLC, thin-layer chromatography.

Running Title: [6]-Shogaol Derivatives as Nrf2 Activators

ABSTRACT:

Oxidative stress is a central component of many chronic diseases. The Kelch-like ECH-associated protein 1 (Keap1)-nuclear factor erythroid 2 p45-related factor 2 (Nrf2) system is a major regulatory pathway of cytoprotective genes against oxidative and electrophilic stress. Activation of the Nrf2 pathway plays crucial roles in the chemopreventive effects of various inducers. In this study, we developed a novel class of potent Nrf2 activators derived from ginger compound, [6]-shogaol (6S), using the *Tg[glutathione S-transferase pi 1 (gstp1):green fluorescent protein (GFP)]* transgenic zebrafish model. Investigation of structure-activity relationships of 6S derivatives indicates that the combination of an *α,β*-unsaturated carbonyl entity and a catechol moiety in one compound enhances the *Tg(gstp1:GFP)* fluorescence signal in zebrafish embryos. Chemical reaction and *in vivo* metabolism studies of the four most potent 6S derivatives showed that both *α,β*-unsaturated carbonyl entity and catechol moiety act as major active groups for conjugation with the sulfhydryl groups of the cysteine residues. In addition, we further demonstrated that 6S derivatives increased the expression of Nrf2 downstream target, heme oxygenase-1, in both a dose- and time-dependent manner. These results suggest that *α,β*-unsaturated carbonyl entity and catechol moiety of 6S derivatives may react with the cysteine residues of Keap1, disrupting the Keap1-Nrf2 complex, thereby liberating and activating Nrf2. Our findings of natural product-derived Nrf2 activators lead to design options of potent Nrf2 activators for further optimization.

Keywords:

[6]-Shogaol derivatives; Metabolism; Nrf2 activators; *Tg(gstp1:GFP)* transgenic zebrafish model

INTRODUCTION

Nuclear factor erythroid-2 related factor 2 (Nrf2), a transcription factor and basic leucine zipper protein, regulates the expression of cytoprotective molecules that counteract against oxidative and electrophilic stress.[1] Under basal conditions, Nrf2 is constantly targeted for Kelch-like ECH-associated protein 1 (Keap1)-mediated ubiquitination and subsequent proteasomal degradation to maintain a low level of Nrf2 protein in the cells. Upon activation in response to oxidative and electrophilic stress, Nrf2 detaches from Keap1, migrates to the nucleus, and binds to the antioxidant response element (ARE) sequence to activate transcription of cytoprotective and detoxifying genes.[2-4] The association of Keap1 with Nrf2 mainly relies on the cysteine residues in the protein Keap1, and the sulfhydryl groups of the cysteine residues are probably the direct sensors of inducers of the phase II system.[5, 6] Therefore, Nrf2 is a potential target for many chronic diseases, such as chronic kidney disease, asthma, neurodegenerative diseases, and cancer.[7-13] It is known that small molecules Nrf2 activators, such as sulforaphane (SFN),[14] curcumin,[15] and chalcone derivatives,[16] have been identified as cancer chemopreventive agents. Screening for Nrf2 activators would lead to the discovery of new pharmaceuticals for oxidative stress-associated chronic diseases.

The Keap1-Nrf2 system is conserved among vertebrates, including zebrafish.[17-19] Zebrafish Nrf2 protein shares six highly conserved Neh domains with mammalian Nrf2 proteins, which are considered to play critical functions in Nrf2 regulation.[20] High sequence identities in each Neh domain between zebrafish and mouse Nrf2 imply a

common regulatory mechanism among vertebrate Nrf2s.[17] This finding justifies zebrafish as a powerful tool to analyze the molecular basis of the Nrf2-Keap1 system. Among the known endogenous targets of zebrafish Nrf2, the pi-class glutathione *S*-transferase 1 gene (*gstp1*) showed the strongest induction in both electrophile-treated and Nrf2-overexpressing embryos, and is regarded as an important determinant for the protection against insults of various electrophilic agents.[21] This gene has also been observed in mammals and humans.[22, 23] A green fluorescent protein (GFP) reporter gene driven by the *gstp1* promoter was created in the *Tg(gstp1:GFP)* transgenic zebrafish line by Dr. Kobayashi's group; the promoter containing an ARE-like sequence located 50 bp upstream of the transcription initiation site was shown to be essential and sufficient for Nrf2 transactivation.[24] Obviously, *Tg(gstp1:GFP)* transgenic zebrafish provides a new and attractive platform to screen novel Nrf2 activators in vivo for drug discovery. A recent study has successfully identified nitro-fatty acids and cyclopentenone prostaglandins as potent Nrf2 activators using the *Tg(gstp1: GFP)* transgenic zebrafish model.[25]

In a recent study, we identified [6]-shogaol (6S), a major component of dry ginger, as an activator of Nrf2 in colon epithelial cells *in vitro* and *in vivo*.[26] Our data obtained with gene expression profiling, Western blotting and immunostaining clearly demonstrated that 6S induced nuclear translocation of Nrf2 and activated Nrf2 target genes in an Nrf2-dependent manner.[27] With an α,β-unsaturated carbonyl group in the alkyl tail, 6S is a typical Michael acceptor. We hypothesized that 6S could activate Nrf2 via alkylation of cysteine residues of Keap1 protein. This was confirmed by our observations that 6S modified Keap1 at 17 cysteine residues and these cysteine residues were located in all 5

domains of Keap1 protein. Keap1 is a cysteine-rich protein possessing 27 cysteine residues in the human protein. Alkylation of one or more of the cysteine residues of Keap1 by xenobiotic electrophiles appears to be an important signaling mechanism for the regulation of ARE activity through Nrf2.[28] These findings prompt us to synthesize a series of 6S derivatives and conduct a structure-activity relationship (SAR) study of 6S derivatives responsible for Nrf2 activation using the *gstp1* reporter transgenic zebrafish model. We designed and synthesized a panel of 6S derivatives (Schemes 1 and 2) to probe their SAR and Nrf2 activation on transgenic zebrafish embryos. We further investigated the formation of cysteine conjugates of representative 6S derivatives in mice and in zebrafish embryos to understand their underlying molecular mechanisms.

MATERIALS AND METHODS

Materials. Anhydrous chemical reactions were carried out in oven-dried glassware under a nitrogen atmosphere unless otherwise noted. Reactions were monitored by analytical thin-layer chromatography (TLC) on 250 μm silica gel plates (GF254) (Merck) and visualized under UV light. The products were isolated and purified by either preparative TLC on 1000 μm silica gel plates (GF254) (Sorbent Technologies, catalog no. 1617124) or column chromatography (CC) using silica gel (Sorbent Technologies, catalog no. 3093M-25). ^{1}H, ^{13}C NMR, and two-dimensional (2-D) NMR spectra were recorded on a Bruker AVANCE 400 MHz or 600 MHz spectrometer (Bruker, Inc., Silberstreifen, Rheinstetten, Germany) using TMS as an internal standard. Chemical shifts (δ) are expressed in ppm. Coupling constants (J) are expressed in Hz, and multiplicities are indicated by s (singlet), d (doublet), t (triplet), q (quartet), and br

(broad). The ^{13}C NMR spectra are proton decoupled. Shogaols (**1–3**) and gingerols (**11–13**) used in the present study were purified from ginger extract.[29] 6S metabolites, **4–10**, **14–17** and **25** were obtained from [6]-shogaol as described in our previous study.[30] Other chemicals were purchased from Sigma-Aldrich (St. Louis, MO) and were used without further purification. All compounds used were > 95% pure. Fetal bovine serum and penicillin/streptomycin were purchased from Gemini Bio-Products (West Sacramento, CA). Human normal colonic epithelial cells (CCD 841 CoN, ATCC® CRL-170TM) were obtained from ATCC (Manassas, VA).

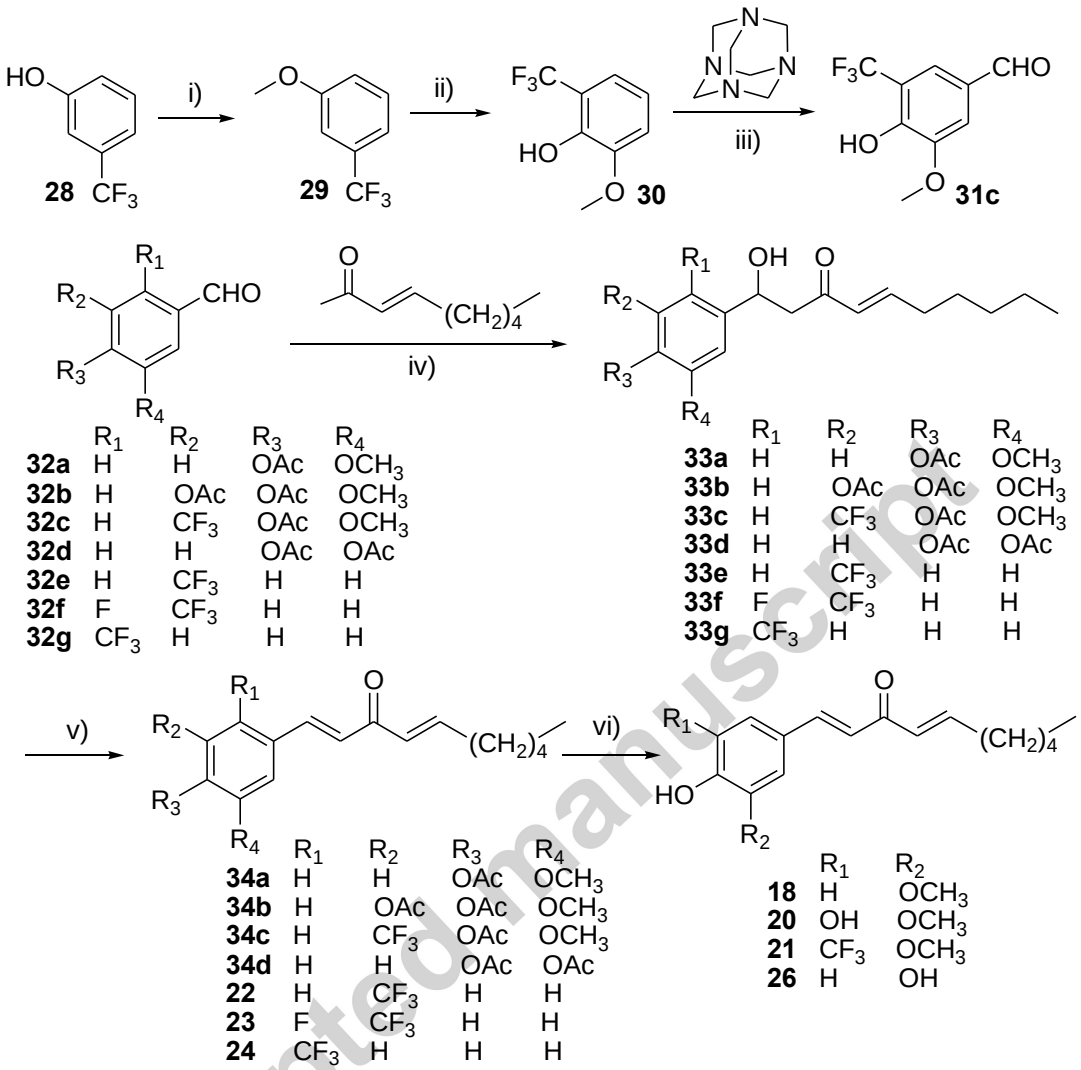

Scheme 1. Synthesis of aldehyde (**31c**) and [6]-dehydroshogaol derivatives (**18, 20-24,** and **26**). Regents and conditions: i) CH_3I, K_2CO_3, acetone, 0 ^oC–rt, 18 h, yield 100%; ii) n-BuLi, THF, -78 ^oC-rt, 25 min; $B(OMe)_3$, -78 ^oC–rt, 18 h; NH_3 in MeOH; and then H_2O_2, 0 ^oC–rt, 2 h, yield 50%; iii) hexamethylenetetramine, TFA, reflux, 3 h, yield 20%; iv) *trans*-3-nonen-2-one, n-BuLi, DIPA, THF, -78 ^oC, 35 min, yield 34–90%; v) PTSA, toluene, reflux, 5 min, yield 36–86%; vi) LiOH, THF/MeOH/H_2O, rt, 5 min, yield 59–83%.

Synthesis of [6]-Shogaol Derivatives. Aryl-1,4-dien-3-ones, typical Michael acceptors, could be synthesized by Horner-Emmons olefination of 2-oxo-3-alkenylphosphonates with benzaldehydes in the presence of lithium bromide and triethylamine,[31] or by conjugate addition of vinyl iodide to styryl-activated enones under n-BuLi.[32, 33] In light of several disadvantages of these procedures including high reactive species required, and the use of expensive or noncommercial available reagents, we herein developed a straightforward and simple strategy to synthesize aryl-dec-1,4-dien-3-ones (6S derivatives), using commercial aromatic aldehydes and low reactive species 3-nonen-2-one via nucleophilic addition and subsequent dehydration. In short, the appropriate substituted aromatic aldehydes (**32a-g**) were treated with lithium species of 3-nonen-2-one to form *β*-hydroxyenones (**33a-g**), and then a rapid PTSA-catalyzed dehydration was followed, furnishing the target [6]-dehydroshogaol derivatives (**18, 20-24** and **26**) (Scheme 1).

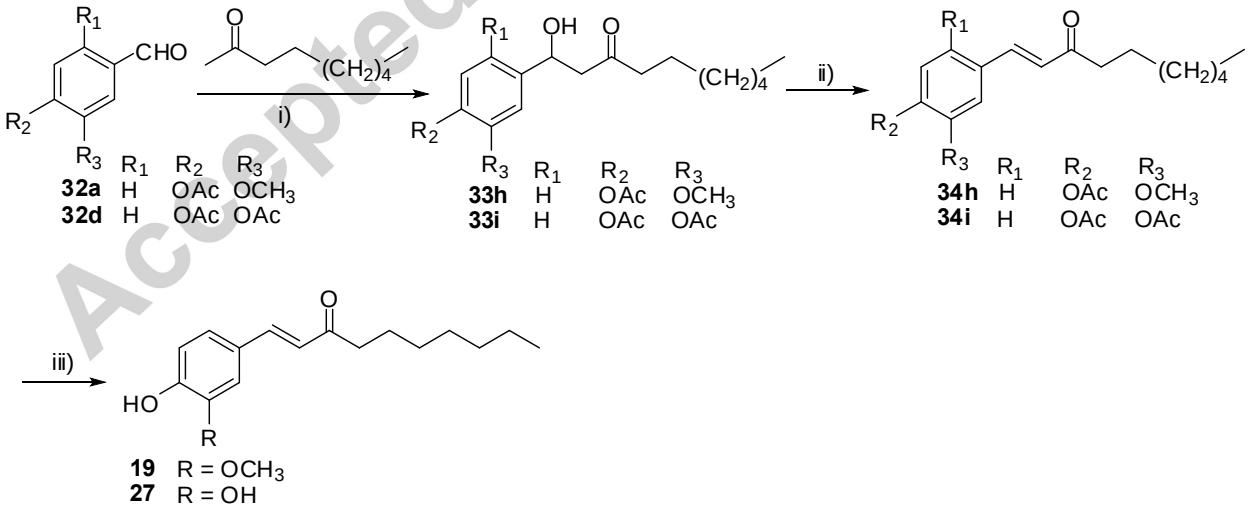

Scheme 2. Synthesis of [6]-dehydroparadol derivatives (**19** and **27**). Regents and conditions: i) 2-nonanone, n-BuLi, DIPA, THF, -78 ^{o}C, 35 min, yield 32–85%; ii) PTSA,

toluene, reflux, 5 min, yield 41–68%; iii) LiOH, THF/MeOH/H_2O, rt, 5 min, yield 79–80%.

Likewise, [6]-dehydroparadol derivatives (**19** and **27**) were successfully prepared using aromatic aldehydes (**32a** and **32d**) and low reactive lithium species of 2-nonanone (Scheme 2). Non-commercially available aldehyde **31c** was prepared from 3-(trifluoromethyl)phenol following the steps as reported in the literature.[34] Cysteinyl conjugates **35** and **36** were readily made under Michael addition condition according to the method for the preparation of cysteine conjugate of 6S (Scheme 3A).[30] Conjugate **37** was successfully synthesized through IBX-mediated oxidation to the *o*-quinone followed by nucleophilic addition of L-cystein (Scheme 3A).[35] The synthesis details and spectroscopic data for these compounds are given in the Supplemental Information and their structures and purity were confirmed by ^{1}H and ^{13}C NMR spectroscopy, and LC-ESI/MS. All final products are > 95% pure.

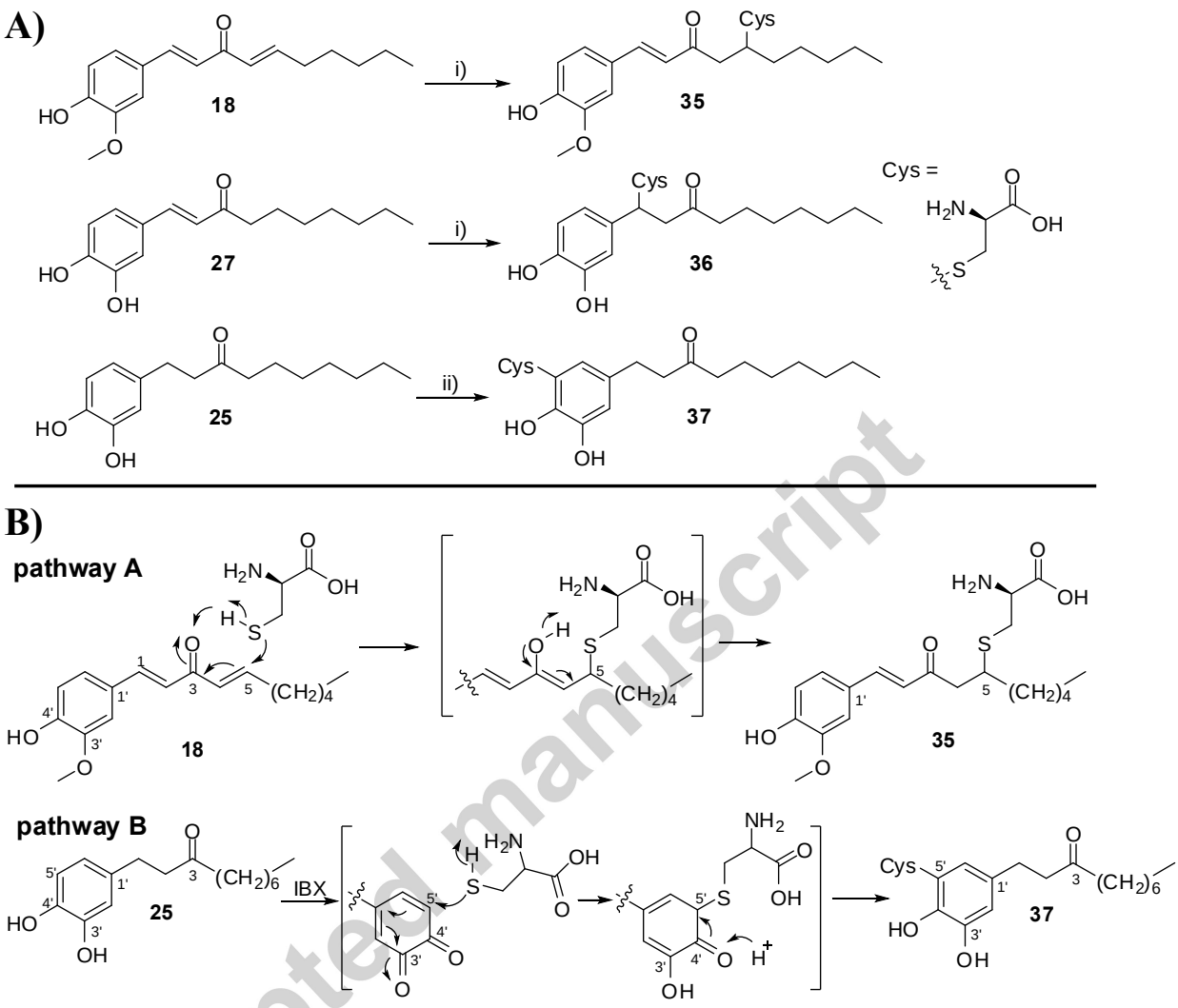

Scheme 3. Synthesis of cysteine conjugates of [6]-shogaol derivatives (**35-37**) (A) and their proposed reaction mechanism (B). Regents and conditions: i) L-cystein, $NaHCO_3$ (cat.), MeOH/PBS (5:1), rt, 10 min, yield 14-39%; ii) L-cysteine, IBX, MeOH/PBS, -78 ^{o}C-rt, 1.5 h, yield 78%.

LC/MS Analysis. LC/MS analysis was carried out with a Thermo-Finnigan Spectra System, which consisted of an Accela high speed MS pump, an Accela refrigerated autosampler, and an LCQ Fleet ion trap mass detector (Thermo Electron, San Jose, CA, USA) incorporated with an electrospray ionization (ESI) interface. A Gemini-NX C_{18}

column (150 mm × 4.6 mm i.d., 5 μm, Phenomenex) was used for separation at a flow rate of 0.3 mL/min. The column was eluted with 100% A (5% aqueous methanol with 0.2% formic acid) for 1 min, followed by linear increases in B (95% aqueous methanol with 0.2% formic acid) to 55% from 1 to 4 min, to 85% from 4 to 25 min, then to 100% B from 25 to 30 min, and then with 100% B from 30 to 35 min. The column was then re-equilibrated with 100% A for 5 min. The LC eluent was introduced into the ESI interface. The positive ion polarity mode was set for the ESI source with the voltage on the ESI interface maintained at approximately 4.6 kV. Nitrogen gas was used as the sheath gas and auxiliary gas. Optimized source parameters, including capillary temperature (260 ^{o}C), sheath gas flow rate (31 arbitrary units), auxiliary gas flow rate (16 units), tube lens (34 V), and capillary voltage 9 V, were tuned using authentic samples. The collision-induced dissociation (CID) was conducted with an isolation width 2 Da and normalized collision energy of 35 for MS^2. The mass range was measured from 100 to 800 *m/z*. Data acquisition was performed with Xcalibur version 2.0 (Thermo Electron, San Jose, CA, USA).

Transgenic Zebrafish and Embryos. Zebrafish AB transgenic strains *Tg(gstp1:GFP)* were maintained in a Pentair Aquatic Ecosystem fish housing unit with 14 h light/10 h dark cycle.[25] The fish embryos were maintained at 28.5 °C in 0.3X Danieau's solution (19.3 mM NaCl, 0.23 mM KCl, 0.13 mM $MgSO_4$, 0.2 mM $Ca(NO_3)_2$, 1.7 mM HEPES, pH 7.0) containing 30 μg/ml phenylthiourea (PTU) to inhibit pigmentation. *Tg(gstp1:GFP)* cross with AB wild-type strain fluorescence embryos were used for the experiment. Zebrafish embryos were washed, dechorionated and anaesthetized before

observations, and fluorescence imaging for analysis. All zebrafish experiments were approved by IACUC committee at the North Carolina Central University.

Chemical Treatments. Transgenic zebrafish embryos at 1 day-post-fertilization (dpf) were dechorionated and placed in Petri dishes containing different chemicals diluted in 0.3X Danieau's solution containing PTU. The chemical stock was dissolved in DMSO at 5 mM concentration. The control contains DMSO at the corresponding concentration of 0.1% which showed no effect on embryonic development and no effect on *Tg(gstp1:GFP)* fluorescence activity.

Fluorescent Imaging. An Olympus MVX10 Fluorescence Macroscope (Olympus, Center Valley, PA) equipped with a Hamamatsu C9300-221 high-speed digital CCD camera (Hamamatsu City, Japan) was used for fluorescence microscopy. *Tg(gstp1:GFP)* fluorescent embryos were anaesthetized in tricaine and imaged at 2 dpf (day-post-fertilization). MetaMorph Basic software (Olympus, Center Valley, PA) was used for image acquisition and analysis.

Quantification of Nrf2 Reporter Activity by *Tg(gstp1: GFP)* Fluoresence in Zebrafish Model. The fluorescence intensity of the olfactory neural epithelia is quantitated using MetaMorph Basic software. In brief, GFP expression in the olfactory regions of *Tg(gstp1:GFP)* embryos treated with various chemicals was measured after 24-hour treatment from 1 dpf to 2 dpf. The GFP induction was detectable by fluorescence signal at the area of the olfactory epithelia in the anterior of the head region, the intensity was measured using an area of a circle of 60 pixel diameter of the fluorescence olfactory epithelia subtracted by a background non-fluorescence area next to the zebrafish embryo.

Both the left and right olfactory epithelia were measured to give an average fluorescence value. The values are an average of measurements from at least 10 embryos.

Measurement of reactive oxygen species (ROS). Zebrafish embryos (20/group) at 1dpf were dechorionated, and treated with 5 μM compounds **1**, **18**, **26**, and **27** over 2, 4, 8, and 24 h. The embryos at each time point were then used for ROS extraction and analysis. The ROS assay employed the cell-permeable fluorogenic probe 2′, 7′-dichlorodihydrofluorescindiacetate [DCFH-DA] (Sigma Aldrich, St. Louis, MO) to measure the relative changes in O^{-}_{2} and H_2O_2 levels in Zebrafish embryos after treatment. All the Zebrafish embryos were homogenized in 400 μL ice-cooled PBS, and 100 μL homogenate was added into the well of 96-well plate in triplicate (PBS was run as background). Each well was added 5 μL 20 mM DCFH-DA stock freshly prepared, and then the plate was incubated at 37 °C for 15, 30, and 60 min. The plate was immediately placed in a Biotek microplate reader to measure fluorescence at wavelengths of 485 (excitation) and 528 (emission) at the given incubation time points. The protein concentrations of homogenate were determined using Bradford method. The corrected fluorescent values were calculated as the increase rate per minute per mg protein and normalized to respective control for each time point and are presented as fold induction (n = 3).

Western Blotting. Human normal colonic epithelial cells (CCD 841 CoN) were grown in Eagle's Minimum Essential Medium with 10% fetal bovine serum and 1% penicillin/streptomycin, and maintained at 37 ^{o}C in a 100% humidified atmosphere of 5% CO_2 and 95% air. Fresh growth medium was added to the cells every two days until

confluent. Cells were planted in 145 × 20 mm flat-bottomed tissue culture dishes and growth to 70-80% confluence and then treated with compound **27** for various doses and time points. At the end of incubation period, cell lysates were prepared in ice-cold Cell Lysis Buffer (Cell Signaling, Danvers, MA) with 1% protease inhibitor cocktail and 1% phenylmethylsulfonyl fluoride (Sigma, St. Louis, MO). Protein concentrations were measured using BCA Protein Assay Kit (Thermo Scientific, Rockford, IL, USA). Aliquots containing 30 μg protein were loaded onto a 10-12% sodium dodecyl sulfatepolyacrylamide gel, transblotted onto polyvinylidene difluoride (PVDF) membrane (Bio-Rad Laboratories, Beverly, CA), blocked with Tris buffered saline with 1% Casein with 0.1% Tween-20, and then incubated with each of the primary antibodies of HO-1 and β-actin overnight at 4 ^{o}C (Cell Signaling, Beverly, MA). The membrane was then incubated with horseradish peroxidase-conjugated donkey anti-rabbit IgG (Cell signaling, Danvers, MA). The bound complexes were detected with SuperSignal Chemiluminescent Substract (Thermo Scientific, Rockford, IL). The immunoblot bands were quantified by densitometry analysis, and the ratio to β-actin was calculated and presented.

Biotransformation of Xenobiotics 18 and 25-27 in Zebrafish Embryos. Zebrafish embryos were staged and maintained according to NCCU IACUC guidelines. In short, fifty zebrafish embryos at the 8 hour-post-fertilization (hpf) stage were incubated at 28.5 ^{o}C in 0.3X Danieau's solution (19.3 mM NaCl, 0.23 mM KCl, 0.13 mM $MgSO_4$, 0.2 mM $Ca(NO_3)_2$, 1.7 mM HEPES, pH 7.0) with or without 5 μM **18** and **25-27**, respectively. At 24 hpf, embryos were dechorionated manually and the chorions were carefully removed one by one from the culture medium. The zebrafish embryos were harvested and kept at -80 ^{o}C till analyze by LC/MS.

Zebrafish Embryo Sample Preparation. 200 μL Sodium acetate buffer solution (pH 5.0) was added to 50 zebrafish embryos. Samples were homogenized for 90 s by an Omni Bead Ruptor Homogenizer (Kennesaw, GA). 10 μL 10% ascorbic acid and 300 μL sodium acetate buffer were added to the homogenates. The mixture was incubated in the presence of β-glucuronidase (250 U) and sulfatase (3 U) at 37 ^{o}C for 45 min, and then 600 μL MeOH with 1% acetic acid was added. The resulting mixture was vortexed for 30 s and then centrifuged at 17000g for 10 min. The supernatant was removed and evaporated under a gentle stream of nitrogen. The residue was reconstituted in 150 μL 90% MeOH with 0.2% AA, and 10 μL was analyzed directly by LC/MS.

Mouse Study. The Institutional Review Board approved the protocol for mouse study through the Animal Care and Facilities Committee at North Carolina Central University. Female C57BL/6J mice were purchased from the Jackson Laboratory (Bar Harbor, ME, USA) and allowed to acclimate for at least 1 week prior to the start of the experiment. The mice were housed 5 per cage and maintained in air-conditioned quarters with a room temperature of 20 ± 2 ºC, relative humidity of 50 ± 10 %, and an alternating 12-h light/dark cycle. Mice were fed Rodent Chow #5001 (LabDiet) and water, and were allowed to eat and drink *ad libitum*. Synthetic compounds **18** and **27** in DMSO were administered to mice by oral gavage (200 mg/kg), respectively. Urine samples were collected in metabolic cages (5 mice per cage) in 24 h after administration. The samples were stored at -80 ºC until analysis.

Mouse Urine Sample Preparation. Enzymatic deconjugation of mouse urine was performed as described previously with slight modifications.[36] In brief, triplicate samples were prepared in the presence of β-glucuronidase (250 U) and sulfatase (3 U) for 1.0 h at

37 ^{o}C. After incubation, 500 μL methanol containing 0.2% AA was added to the medium. The resulting suspension was centrifuged at 17,000 g for 5 min, and 10 μL of supernatant was analyzed directly by LC/MS.

Statistical analysis. All results are presented as means ± standard deviation. An unpaired *t* test was used to determine potential differences between each treatment and control. Comparisons between all treatments and control were measured by one way ANOVA with Dunnett's test using the GraphPad Prism version 5.04. A *p* value of less than 0.05 was considered statistically significant in all tests.

RESULTS AND DISCUSSION

Potency of 6S Derivatives to Activate Nrf2 in Transgenic Zebrafish Embryos. We have previously identified Nrf2 as a molecular target of ginger compound 6S in colon epithelial cells *in vitro* and *in vivo*.[27] In the current study, we found that 6S (**1**) is even more active than SFN (2.40 vs. 2.03 times higher than vehicle) (Figure 1), a well-known potent activator of Nrf2.[37, 38] Using quantitative microscopy, we showed GFP fluorescence intensity at the olfactory sensory neural epithelia of 6S-treated zebrafish embryos is stronger than those of SFN-treated individuals (Figure 2). We hypothesized that the α,β-unsaturated carbonyl entity in the side chain of 6S plays a pivotal role for Nrf2 activation.

To test our hypothesis, we compared the activity of 6S with its derivatives with the conversion of ketone group into hydroxyl group (**4**), the reduction of olefinic double bond (**5**), or both (**14**), as well as their related derivatives (**6**-**10** and **15**-**17**). Our results clearly indicate that the departure of the α,β-unsaturated carbonyl entity attenuated Nrf2-induced activities (Figure 1). 6S demonstrated stronger activity than compounds **4** (1.13 times

higher than vehicle) and **5** (1.27 times higher than vehicle), and compound **14** had no effect at all (Figure 1). Furthermore, thiol conjugation (**6**-**9**) also diminished the activity of 6S. 6G (**11**), the hydrated precursor of 6S, was also less potent than 6S (1.87 vs. 2.40 times higher than vehicle). We further determined how the side chain length affected the activity of 6S by comparing the effects of 6-, 8-, and 10S (**1**-**3**) in *Tg(gstp1: GFP)* transgenic zebrafish embryos. Our results indicate that their activities are in the order of 6S > 8S > 10S (2.40 vs. 1.67 vs. 1.53) (Figure 1). A similar result was obtained for 6-, 8-, and 10G (**11**-**13**) (1.87 vs. 1.65 vs. 1.29) (Figure 1). This suggests that the lipophilicity of the alkyl tails in 6S derivatives diminishes the potency. Taken together, our results supported that a central core consisting of an α,β-unsaturated carbonyl entity and a ten-carbon units of alkyl tail in 6S derivatives would exert a potent Nrf2 activation and could serve as core structures to further develop novel Nrf2 activators.

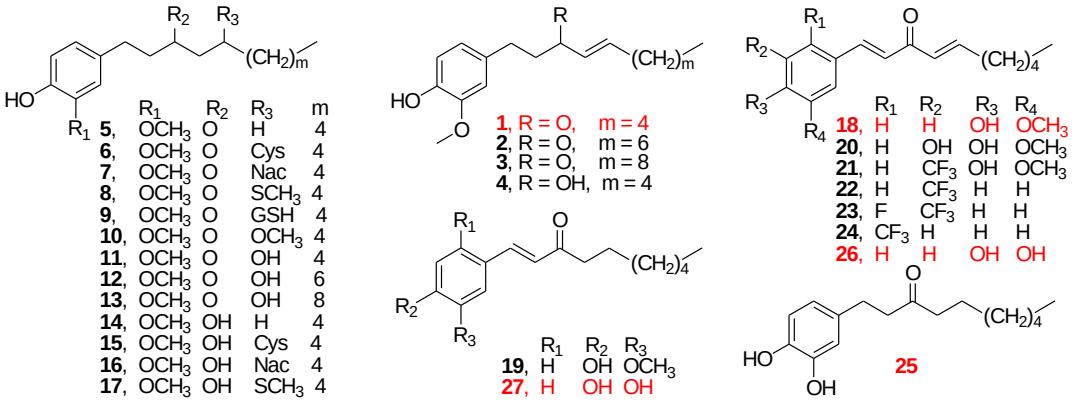

Compound ID	Ratio/CTL
DMSO	1.00
SFN	2.03 ± 0.49
1	2.40 ± 0.54
2	1.67 ± 0.55
3	1.53 ± 0.53
4	1.13 ± 0.21
5	1.27 ± 0.29
6	1.06 ± 0.20
7	1.04 ± 0.05
8	1.16 ± 0.47
9	0.93 ± 0.21
10	0.96 ± 0.24
11	1.87 ± 0.51
12	1.65 ± 0.29
13	1.29 ± 0.40

Compound ID	Ration/CTL
14	0.96 ± 0.21
15	1.08 ± 0.65
16	0.78 ± 0.12
17	0.72 ± 0.14
18	5.67 ± 0.59
19	3.29 ± 0.35
20	1.26 ± 0.14
21	2.18 ± 0.53
22	1.28 ± 0.10
23	1.63 ± 0.17
24	1.55 ± 0.67
25	4.32 ± 0.50
26	6.96 ± 0.48
27	9.19 ± 0.12

Figure 1. Structures of compounds **1-27** and their effects on *Tg(gstp1:GFP)* fluorescence signal in the *Tg*(*gstp1:GFP)* transgenic zebrafish embryos at a concentration of 5 μM. The induced activities are indicated by the ratios of GFP fluorescence intensities in 6S derivatives treatment to control. The values are expressed as the mean ± SD (n = 3-7). CLT, DMSO control; GFP, green fluorescent protein; SFN, sulforaphane.

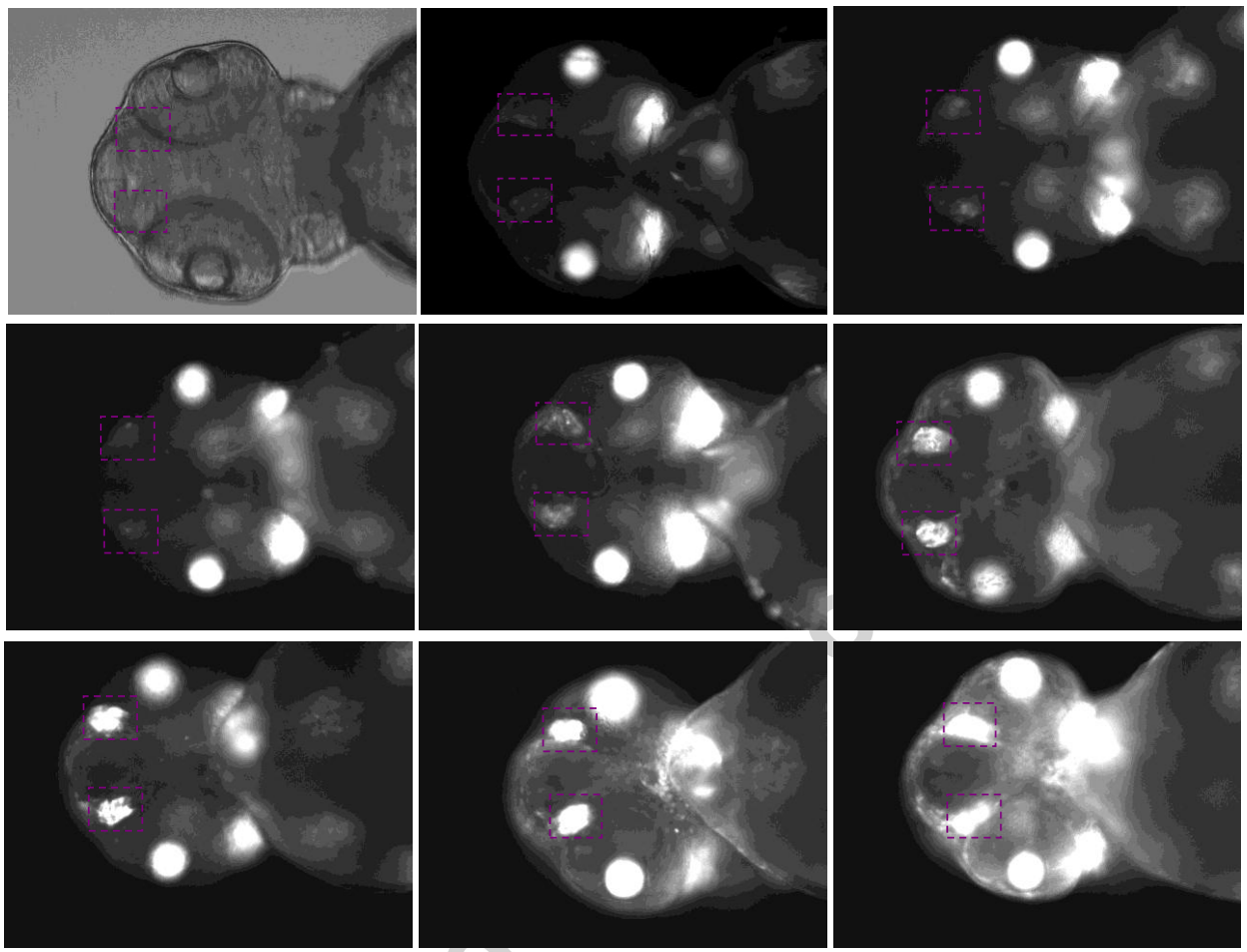

Figure 2. *Tg(gstp1:GFP)* fluorescence signal at the olfactory sensory neural epithelia of zebrafish embryos at 2 day after 24 hr treatment with compounds **1**, **11**, **18**, and **25-27**, at a concentration of 5 μM. Top left is the bright field image of control (CTL) at the ventral view of head region, the rest are fluorescent images of GFP signal. The inducible *Tg(gstp1:GFP)* activity at the olfactory sensory neural epithelia was indicated by the two rectangles. GFP, green fluorescent protein; 6G, [6]-gingerol; 6S, [6]-shogaol; SFN, sulforaphane.

Recent studies have revealed that conjugated enones such as chalcones can stimulate expression of Nrf2-dependent genes such as HO-1, NQO-1, and GCLM, and are potent

Nrf2 activators *in vitro* and *in vivo*.[16, 21, 39] We therefore designed and synthesized conjugated 6S derivatives **18** and **19** (Schemes 1 and 2). We observed that both compounds **18**, with a 1-aryl-1,4-dien-3-one entity in the structure, and **19**, with a 1-aryl-1-en-3-one entity in the structure, were more potent than 6S (5.67 vs. 2.40 and 3.29 vs. 2.40), suggesting that conjugated unsaturated ketones in the side chains of 6S derivatives greatly favor the activation of Nrf2.

Aside from the chemical modifications on the side chain, the electronic properties of the substituents on the aromatic rings of 6S derivatives were investigated. Firstly, we observed that an extra electron-donating group (-OH) at the C-5' position of the aromatic ring in **18**, corresponding to **20** (Scheme 1), diminished the activity of **18** (1.26 vs. 5.67) (Figure 1). Similarly, the introduction of an electron-withdrawing group (-CF_3) into the C-5' position of the ring in **18**, corresponding to **21** (Scheme 1), also weakened the activity of **18**, but had better activity than **20** (2.18 vs. 1.26). We also observed that the removal of the hydroxyl and methoxyl groups from **21**, corresponding to **22**, further decreased the efficacy of **21** (1.28 vs. 2.18). Adding another electron-withdrawing group (-F) into the C-6' position of the ring in **22**, corresponding to **23** (Scheme 1), or changing the substitution position of -CF_3, corresponding to **24** (Scheme 1), only slightly increased the activity of **22** (1.63 vs. 1.28 and 1.55 vs. 1.28) (Figure 1).

Interestingly, we noticed that derivative **25**, a metabolite of 6S,[40] containing a catechol moiety and an isolated ketone group in the structure, exerted a comparable potency (4.32 times higher than vehicle) to conjugated enone **18** (5.67 times higher than vehicle) (Figures 1 and 2). This indicates that a catechol moiety in the structure is as essential as an α,β-unsaturated carbonyl entity for Nrf2 activation. Inspired by the

observation from catechol **25**, we combined a catechol moiety and an unsaturated carbonyl entity in a molecule, eventually resulting in the synthesis of complexes of catechol and conjugated enone **26** and **27** (Schemes 1 and 2). In the end, we observed that both **26** and **27** showed enhanced Nrf2-induced activity (6.96 times higher than vehicle for **26**; and 9.19-fold higher than vehicle for **27**), and are more active than conjugated enone **18** (5.67 times higher than vehicle), **19** (3.29 times higher than vehicle), and catechol **25** (4.32 times higher than vehicle) (Figures 1 and 2). Interestingly, the activity of **27** is higher than the sum of **25** (4.32 times higher than vehicle) and **19** (3.29 times higher than vehicle), and the activity of **26** (6.96 times higher than vehicle) is also higher than **25** and **18**. These findings suggest that the combination of a catechol moiety and a conjugated enone improves the Nrf2-induced activity.

Taken together, we identified four 6S derivatives **18** and **25-27** as potent Nrf2 activators in transgenic zebrafish embryos for the first time. Investigation on SAR of 6S derivatives demonstrated that 1) an α,β-unsaturated carbonyl entity in the alkyl tail is crucial for Nrf2 activation; 2) a conjugated unsaturated ketone in the structure enhances the activity; 3) a catechol moiety in the structure plays a pivotal role in Nrf2-induced activities; and 4) coexistence of a catechol moiety and a conjugated unsaturated ketone in one molecule improves the activity.

Effects of 6S and Its Derivatives (18, 26, and 27) on Cellular ROS Levels. In order to determine whether ROS plays a role in the activation of Nrf2 pathway, we measured the cellular ROS levels in zebrafish embryos treated with test agents at 2, 4, 8, and 24 h. Our results clearly indicated that these compounds did not induce oxidative stress (Figure

3), suggesting that ROS production is not one of the mechanism of actions of these derivatives.

6S Derivative (27) Increased HO-1 Expression in CCD 841 CoN Cells in Both a Dose- and Time-Dependent manner. To assess the role of 6S derivatives on the induction of Nrf2 downstream genes, human normal colonic epithelial cells CCD 841 CoN were treated for 24 h with compound **27**, the most active 6S derivative to activate Nrf2 in transgenic zebrafish embryos, at different doses of 5, 10, and 20 μM. As shown in Figure 4A, **27** significantly increased HO-1 protein expression, compared to untreated control ($p < 0.05$ for all concentrations). These data clearly illustrate that the representative 6S derivative **27** induces HO-1 expression in CCD 841 CoN cells in a dose-dependent manner.

On the other hand, CCD 841 CoN cells were treated for 3, 6, 12, and 24 h with compound **27** at a dose of 10 μM. As seen in Figure 4B, **27** significantly increased HO-1 expression from time point of 3 h to 24 h when compared to control ($p < 0.05$ for all time points). These observations demonstrate that derivative **27** increases HO-1 expression in CCD 841 CoN cells in a time-dependent manner.

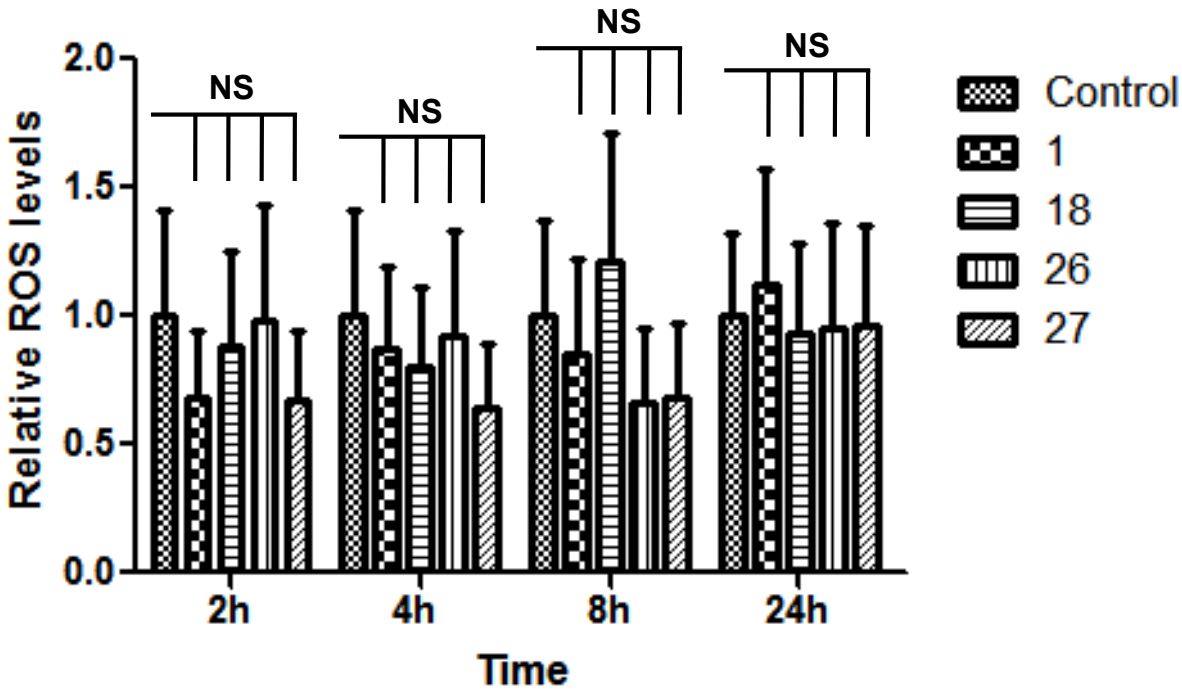

Figure 3. Effects of ROS productions in zebrafish embryos by compounds **1**, **18**, **26** and **27**. Zebrafish embryos at 1 dpf were treated with compounds **1**, **18**, **26**, and **27** at 5 μM over 2, 4, 8, and 24 h, and ROS levels in the embryos at each time point were measured using a cell-permeable fluorogenic probe DCFH-DA. One way ANOVA following Dunnett's test was utilized to determine the potential differences between all treatments and control. NS: no significant difference. ROS, reactive oxygen spicies.

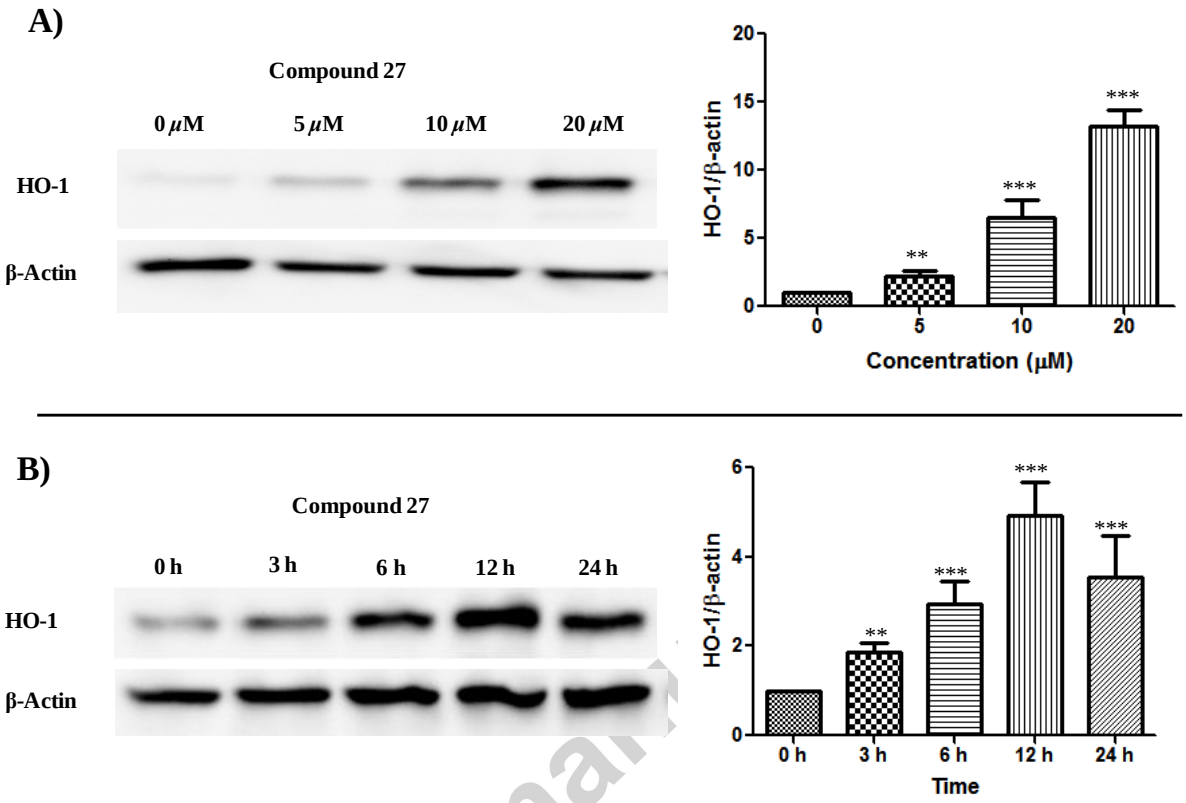

Figure 4. Effects of compound **27** on HO-1 expression in human normal colonic epithelial cells CCD-841CoN. (A) Compound **27** increased HO-1 expression in a dose-dependent manner. Cells were treated with **27** at concentrations of 0, 5, 10, and 20 μM for 24 h, resectively. (B) Compound **27** increased HO-1 expression in a time-dependent manner. Cells were treated by **27** at 10 μM for 0, 3, 6, 12, and 24 h, respectively. β-Actin was used as an internal control. The fold changes in HO-1 expression are shown on the right at each row using densitometric analyses of the bands. Results are mean ± SD (n = 3). Bar, standard error; *, $p < 0.05$; **, $p < 0.01$; ***, $p < 0.001$. all statistical tests are unpaired Student's t test, two-tailed, compared to control (0 μM or 0 h).

Chemical Reactivity of Three Representative 6S Derivatives (18, 25, and 27) with L-Cysteine. It has been reported that reaction of the reactive cystine residues of Keap1

with electrophiles results in the formation of intermolecular disulfide bridges, thus covalently linking two monomers of Keap1, thereby liberating Nrf2.[5] Natural Nrf2/ARE activators such as xanthohumol, isoliquiritigenin, and SFN, all containing electrophilic groups as Michael acceptor, have been reported to react with the cysteine residues of human Keap1.[6, 41] To understand the underlying mechanisms that the newly synthesized 6S derivatives activate Nrf2, we first investigated the chemical reactivity of three representative Nrf2 activators (**18**, **25**, and **27**) with L-cysteine *in vitro*. Similar to the reaction between 6S and L-cysteine,[30] Michael addition reactions between enone **18** or **27** and L-cysteine occurred immediately under slightly basic condition, thereby in 10 min giving rise to respective cysteine conjugates **35** and **36**, both with a cysteine residue attached to the side chain (Scheme 3A). Regarding catechol compound **25**, no Michael addition took place under the same conditions as above because of the absence of an unsaturated carbonyl entity as a Michael acceptor in the structure. Under oxidative environments (i.e. IBX), reaction between **25** and L-cysteine, however, efficiently produced cysteine conjugate **37**, a compound with a cysteine residue binding to the aromatic ring (Scheme 3A), which is consistent with previous observations from the reaction of plant catechol, piceatannol.[35] In addition, treatment of **25** with L-cysteine by tyrosinase from mushroom in PBS generated cysteine conjugate **37** as well (Data not shown).

Thus, we perceived that 1) electrophilic alkenes of α,β-unsaturated carbonyl entities in conjugated enones act as Michael acceptors and undergo Michael addition by nucleophilic sulfhydryl groups of cysteine residues under basic conditions, as indicated in pathway A (Scheme 3B); and 2) high susceptibility of catechol moiety in the structure

under oxidative environments leads to the formation of *o*-quinones as reactive Michael acceptors and subsequently Michael additions take place at *ortho*-position of the catechol groups by the treatment of cysteine residues, as described in pathway B (Scheme 3B). As a result, we identified that both α,β-unsaturated carbonyl entities and catechol moieties in molecules act as major active groups for the assaults of the sulfhydryl groups of the cysteine residues.

Table 1. Cysteine conjugates found in mice and in zebrafish embryos after treatment of xenobiotics **18** and **25-27**, respectively.

No.	RT (min)	$[M + H]^+$	MS/MS
35	22.0	396	**396**/378, 275 $[M - Cys + H]^+$ (B)
36	21.2	384	**384**/263 $[M - Cys + H]^+$
36a	22.8	386	**386**/265 $[M - Cys + H]^+$ (B), 137
37	24.0	384	**384**/367 $[M - NH_2 + H]^+$ (B), 295 $[M - C_3H_7NO_2 + H]^+$, 277, 169
37a	25.2	384	**384**/367, 295 $[M - C_3H_7NO_2 + H]^+$ (B), 267, 167
37b	25.1	386	**386**/368 $[M - H_2O + H]^+$ (B), 351, 297 $[M - C_3H_7NO_2 + H]^+$, 279
38	19.6	382	**382**/261 $[M - Cys + H]^+$

Cys, cysteine; RT, retention time.

*Structural Confirmation of Cysteine Conjugates (**35-37**) Obtained from the Corresponding Chemical Reaction*. Similar to cysteine conjugate of 6S,[30] compound **35** was indicated as the cysteine conjugate of dienone **18**. The attachment of the cysteine

residue at C-5 position in the alkyl tail of **18** was established by HMBC correlations between C-5 (δ_C 42.0) and H_{Cys}-β (δ_H 3.22/2.89) and H-6 (δ_H 1.63) as well as H-4 (δ_H 3.36/2.98) (Figure 5). This is supported by observing *m/z* 275 $[M - Cys + H]^+$ (lose of cysteine moiety from *m/z* 396, pattern a) as the major product ion in its MS/MS spectrum (Table 1 and Figure 5). Therefore, compound **35** was identified as 5-*S*-cysteinyl-[6]-dehydroparadol (Figure 5). Likewise, the interpretation of NMR data identified **36** as 1-*S*-cysteinyl-1-(3,4-dihydroxyphenyl)decan-3-one, which was further confirmed by observing *m/z* 263 $[M - Cys + H]^+$ (lose of cysteine moiety from *m/z* 384, pattern a) as the major product ion in its MS/MS spectrum (Table 1). The ^{1}H NMR and ^{13}C NMR spectra of conjugate **37** were similar to those of **36**, indicating **37** is a cysteine conjugate of **25**. The major differences between **36** and **37** were 1) only two aromatic protons at δ_H 6.82 (1H, brs) and δ_H 6.66 (1H, brs) remained in **37**, and 2) signals for thio-methine (-CH-S-) disappeared in **37**. This suggested that the cysteine residue in **37** is bound to the aromatic ring rather the alkyl tail. The linkage of the cysteine residue at C-5' position of the catechol moiety was accomplished by HMBC correlations between C-3' (δ_C 119.2) and H_{Cys}-β (δ_H 3.47/2.95) (Figure 5B). This was further supported by its MS/MS fragment ions at *m/z* 295 originated from the cleavage of $C_{Cys-\beta}$-S bond (pattern b), and *m/z* 169 formed by the cleavage of $C_{Cys-\beta}$-S bond followed by the α-cleavage of carbonyl group between C_2-C_3 bond (Figure 5C). Compound **37** was therefore identified as 3'-*S*-cysteinyl-1-(3,4-dihydroxyphenyl)decan-3-one (Figure 5A).

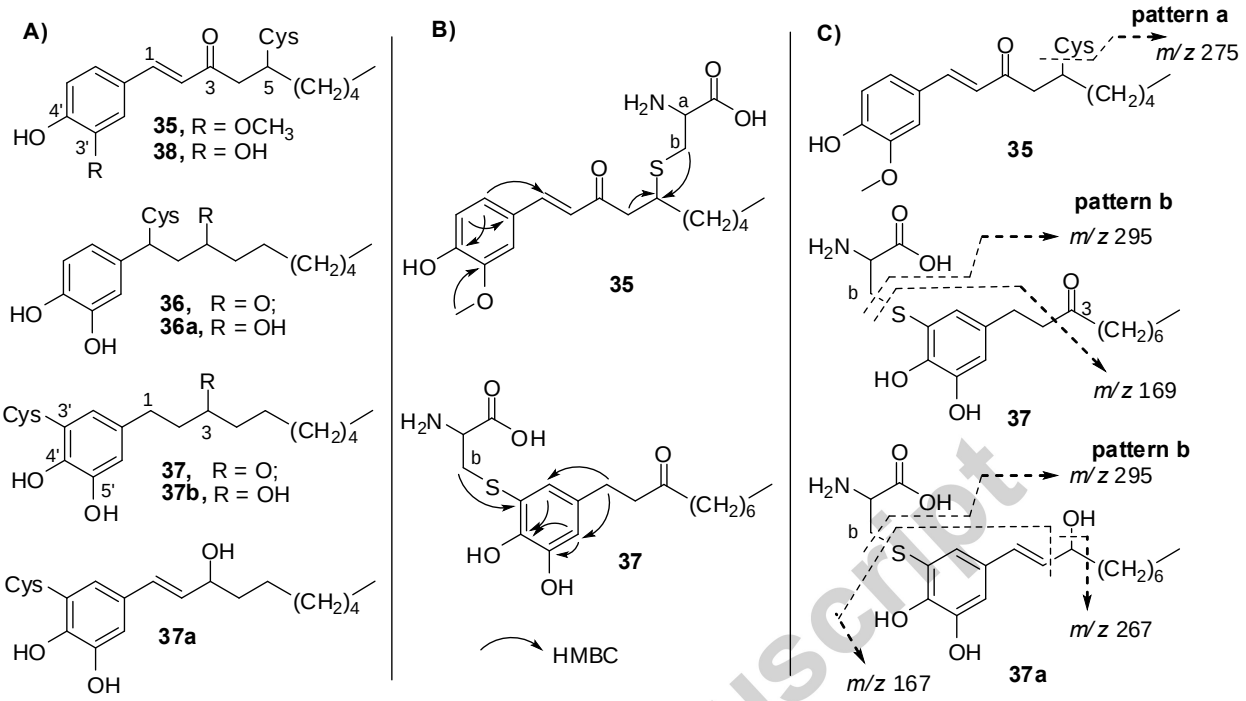

Figure 5. Cysteine conjugates found in mice and in zebrafish embryos. A) Structures of all cysteine conjugates **35**, **36**, **36a**, **37**, **37a**, **37b,** and **38**. B) Main HMBC correlations in the structures of **35** and **37**, respectively. C) Typical fragmentation patterns of **35**, **37**, and **37a** in their respective MS/MS spectra.

Formation of Cysteine Conjugates of 18 and 25-27 in Mice and in Zebrafish Embryos. We have proved that the major active 6S derivatives could bind to the reactive cysteine residues to form related cysteine conjugates *in vitro*. Whether 6S derivatives undergo the similar pathway *in vivo* remains unknown. In this section, **18** and **27** were administrated to mice by oral gavage and **18** and **25-27** were given to zebrafish embryos in incubation medium. We discovered seven cysteine conjugates, including three conjugates (**35-37**) that have been above identified *in vitro* and four new analogues (**36a**, **37a**, **37b**, and **38**), using LC-MS approaches (Figure 5). As shown in Figure 6, conjugate **35** was predominantly present in both mouse urine and zebrafish embryos after treatment

of **18** (Figures 6A and 6B). Besides conjugate **36** and its reduced form **36a**, three additional conjugates **37**, **37a,** and **37b**, with cysteine residue binding to the aromatic ring, were detected from **27**-treated mouse urine (Figure 6C). Likewise, four cysteine conjugates **36**, **36a**, **37,** and **37b** were found in **27**-treated zebrafish embryos (Figure 6D). As expected, conjugates **37** and **37b** were exclusively identified in **25**-treated zebrafish embryos (Figure 6E). Also, three conjugates **37**, **37b,** and **38** were detected in **26**-treated zebrafish embryos (Figure 6F). These *in vivo* observations demonstrated that 1) unsaturated carbonyl entities in the molecules lead to cysteine conjugation occurring on the alkyl side chain, evidenced by the presence of conjugates **35** in **18**-treated mice and zebrafish, **36** and **36a** in **27**-treated mice and zebrafish, and **38** in **26**-treated zebrafish; 2) catechol moieties in the structures induce the binding of cysteine residues to the aromatic rings, evidenced by the appearance of conjugates **37** and **37b** in both **25**- and **26**-treated zebrafish, and **37**, **37a,** and **37b** in **27**-treated mice and zebrafish; and 3) coexistence of unsaturated carbonyl entities and catechol moieties in a molecule leads to the formation of both conjugations, evidenced by the existence of conjugates **37**, **37b,** and **38** in **26**-treated zebrafish, and **36**, **36a**, **37**, **37a,** and **37b** in **27**-treated mice and zebrafish. These *in vivo* results verified that both α,β-unsaturated carbonyl entities and catechol moieties in the molecules act as major active sites for the conjugation with the reactive cysteine residues under physiological conditions.

We have reported that 6S could activate Nrf2 via modification of Keap1 at 17 cysteine residues and these cysteine residues were located in all 5 domains of Keap1 protein.[26] In light of our findings above, we proposed that both α,β-unsaturated carbonyl entities and catechol moieties in 6S derivatives could react with the reactive sulfhydryl

groups of cysteine residues of Keap1, disrupting the Keap1-Nrf2 complex in the cytoplasm, thereby releasing Nrf2. However, this needs to be proved experimentally.

*Structural Elucidation of Cysteine Conjugates (**35-38, 36a, 37a** and **37b**) in Mice and in Zebrafish Embryos by LC/MS.* The presence of conjugates **35-37** in mice and in zebrafish embryos was confirmed by comparison of their retention times and MS/MS fragmentation patterns to those of authentic references obtained from the chemical reactions between corresponding 6S derivatives and L-cysteine (Table 1 and Figure 6). The molecular ion of **36a** at *m/z* 386 $[M + H]^+$ was two units higher than that of **36**, indicating **36a** is the reduced form of **36**. Major fragment ion at *m/z* 265/386 $[M – Cys + H]^+$ in its MS/MS spectrum (Table 1), corresponding to the loss of a cysteine moiety from parent ion at *m/z* 386 (pattern A), suggests that **36a** is 1-*S*-cysteinyl-1-(3,4-dihydroxyphenyl)decan-3-ol (Figure 5A). Compound **37a** had a same molecular ion at *m/z* 384 $[M + H]^+$ (263 + 121) to that of **37**, indicating **37a** is an isomer of **37**. The major MS/MS fragment ion at *m/z* 295 in **37a**, originating from the cleavage of $C_{Cys\text{-}\beta}$-S bond (pattern B), demonstrated the cysteine residue in **37a** is bound to the aromatic ring. Fragment at *m/z* 167 in **37a**, forming by the cleavage of $C_{Cys\text{-}\beta}$-S bond followed by the α-cleavage of carbonyl group between C_2-C_3 bond, was two units less than ion at *m/z* 169 in **37**, suggesting an extra double bond is present in **37a**. This was also supported by ion peak at *m/z* 267, corresponding to the α-cleavage of hydroxyl group between C_3-C_4 bond followed by a loss of H_2O (Figure 5C). Taken together, compound **37a** was proposed as an allyl alcohol isomer of **37**, 3'-*S*-cysteinyl-1-(4,5-dihydroxyphenyl)decen-3-ol (Figure 5A). The molecular weight of compound **37b** (*m/z* 386 $[M + H]^+$) is two units higher than that of **37**, indicating **37b** is a reduced product of **37**. The major MS/MS fragment at *m/z*

297, corresponding to the cleavage of $C_{Cys\text{-}\beta}$-S bond (pattern b) (Table 1), suggested that cysteine residue in **37b** is attached at the aromatic ring. Thus, compound **37b** was tentatively proposed as 3'-*S*-cysteinyl-1-(4,5-dihydroxyphenyl)decan-3-ol (Figure 5A). Compound **38**, found in **26**-treated zebrafish embryos (Figure 6F), had a molecular ion at *m/z* 382 $[M + H]^+$ (261 + 121), indicating **38** is a cysteine conjugate of **26**. The major MS/MS fragment ion at *m/z* 261 (lose of cysteine moiety from *m/z* 382, pattern a) (Table 1) suggested **38** is 5-*S*-cysteinyl-1-(3,4-dihydroxyphenyl)decen-3-one (Figure 5A).

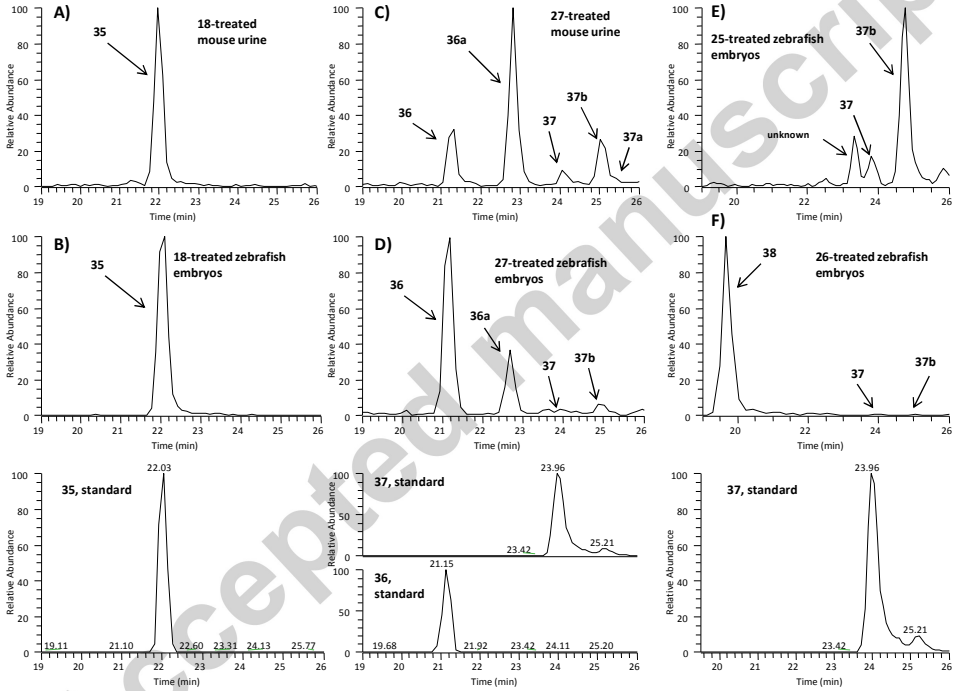

Figure 6. Extracted ion chromatograms of **18**-treated mouse urine (A), **18**-treated zebrafish embryos (B), **27**-treated mouse urine (C), **27**-treated zebrafish embryos (D), **25**-treated zebrafish embryos (E), and **26**-treated zebrafish embryos (F), as well as authentic standards **35**-**37** obtained by positive ESI/MS interface.

CONCLUSION

We have designed, synthesized, and characterized a novel class of 6S derivatives in this study. We, for the first time, identified four compounds, **18** and **25-27,** as the most potent Nrf2 activators using an *in vivo Tg(gstp1: GFP)* transgenic zebrafish embryos model. Study on SAR of 6S derivatives unveiled that 1) an α,β-unsaturated carbonyl entity in the alkyl tail is crucial for Nrf2 activation; 2) a catechol moiety as the ring system of derivatives plays a pivotal role in Nrf2-inducing activities; and 3) coexistence of a catechol moiety and an unsaturated ketone in a molecule improves the activities. Investigation on the chemical reactivity of three representative Nrf2 activators **18**, **25,** and **27**, identified both α,β-unsaturated carbonyl entities and catechol moieties in the molecules as major active sites for the conjugation with the sulfhydryl groups of the cysteine residues *in vitro*. Metabolism of four potent Nrf2 activators, **18** and **25-27**, in mice and in zebrafish embryos demonstrated that 1) unsaturated carbonyl entities in the molecules lead to the conjugation of cysteine residue to the alkyl side chain; 2) catechol moieties in the structures induce the binding of cysteine residues to the aromatic ring; and 3) coexistence of unsaturated carbonyl entities and catechol moieties in a molecule leads to the conjugation at both the alkyl side chain and the aromatic ring. These *in vivo* results further support that both α,β-unsaturated carbonyl entity and catechol moiety act as major active sites for the attacks of the reactive cysteine residues under physiological conditions. Our findings suggest that the reactive cysteine residues of Keap1 may effectively react with these two active sites in 6S derivatives. Therefore, it is worthwhile to further determine the interaction between these derivatives and the cysteine residues of Keap1. In addition, it is also a topic of future study to determine the balance between efficacy and toxicity of these derivatives.

Notes

The authors declare no competing financial interest.

ACKNOWLEDGMENTS

We thank Dr. Makoto Kobayashi at University of Tsukuba for the *Tg(gstp1:GFP)* transgenic zebrafish. We are thankful to Ms. Xiaoyan Huang and Chunyu Xu for the animal care and management of the zebrafish facility.

Appendix A. Supporting Information

Supplementary data associated with this article can be found in the online version.

REFERENCES

(1) Ma, Q. (2013) Role of nrf2 in oxidative stress and toxicity. *Annu. Rev. Pharmacol. Toxicol. 53*, 401-426.

(2) Kensler, T. W., Wakabayashi, N., and Biswal, S. (2007) Cell survival responses to environmental stresses via the Keap1-Nrf2-ARE pathway. *Annu. Rev. Pharmacol. Toxicol. 47*, 89-116.

(3) Sussan, T. E., Rangasamy, T., Blake, D. J., Malhotra, D., El-Haddad, H., Bedja, D., Yates, M. S., Kombairaju, P., Yamamoto, M., Liby, K. T., Sporn, M. B., Gabrielson, K. L., Champion, H. C., Tuder, R. M., Kensler, T. W., and Biswal, S. (2009) Targeting Nrf2 with the triterpenoid CDDO-imidazolide attenuates cigarette smoke-induced emphysema and cardiac dysfunction in mice. *Proc. Natl. Acad. Sci. U. S. A. 106*, 250-255.

(4) Zhang, D. D. (2006) Mechanistic studies of the Nrf2-Keap1 signaling pathway. *Drug. Metab. Rev. 38*, 769-789.

(5) Wakabayashi, N., Dinkova-Kostova, A. T., Holtzclaw, W. D., Kang, M. I., Kobayashi, A., Yamamoto, M., Kensler, T. W., and Talalay, P. (2004) Protection against electrophile and oxidant stress by induction of the phase 2 response: fate

of cysteines of the Keap1 sensor modified by inducers. *Proc. Natl. Acad. Sci. U. S. A. 101*, 2040-2045.

(6) Hu, C., Eggler, A. L., Mesecar, A. D., and van Breemen, R. B. (2011) Modification of keap1 cysteine residues by sulforaphane. *Chem. Res. Toxicol. 24*, 515-521.

(7) Saw, C. L., Wu, Q., and Kong, A. N. (2010) Anti-cancer and potential chemopreventive actions of ginseng by activating Nrf2 (NFE2L2) anti-oxidative stress/anti-inflammatory pathways. *Chin. Med. 5*, 37-43.

(8) Wilson, A. J., Kerns, J. K., Callahan, J. F., and Moody, C. J. (2013) Keap calm, and carry on covalently. *J. Med. Chem. 56*, 7463-7476.

(9) Al-Sawaf, O., Clarner, T., Fragoulis, A., Kan, Y. W., Pufe, T., Streetz, K., and Wruck, C. J. (2015) Nrf2 in health and disease: current and future clinical implications. *Clin. Sci. (Lond) 129*, 989-999.

(10) Choi, B. H., Kang, K. S., and Kwak, M. K. (2014) Effect of redox modulating NRF2 activators on chronic kidney disease. *Molecules 19*, 12727-12759.

(11) Li, Y. J., Kawada, T., and Azuma, A. (2013) Nrf2 is a protective factor against oxidative stresses induced by diesel exhaust particle in allergic asthma. *Oxid. Med. Cell. Longev. 2013*, 323607.

(12) Johnson, D. A., and Johnson, J. A. (2015 (*in press*)) Nrf2-a therapeutic target for the treatment of neurodegenerative diseases. *Free Radic. Biol. Med.*

(13) Kensler, T. W., Egner, P. A., Agyeman, A. S., Visvanathan, K., Groopman, J. D., Chen, J. G., Chen, T. Y., Fahey, J. W., and Talalay, P. (2013) Keap1-nrf2 signaling: a target for cancer prevention by sulforaphane. *Top. Curr. Chem. 329*, 163-177.

(14) Elhalem, E., Recio, R., Werner, S., Lieder, F., Calderon-Montano, J. M., Lopez-Lazaro, M., Fernandez, I., and Khiar, N. (2014) Sulforaphane homologues: Enantiodivergent synthesis of both enantiomers, activation of the Nrf2 transcription factor and selective cytotoxic activity. *Eur. J. Med. Chem. 87C*, 552-563.

(15) Pandey, M. K., Kumar, S., Thimmulappa, R. K., Parmar, V. S., Biswal, S., and Watterson, A. C. (2011) Design, synthesis and evaluation of novel PEGylated

curcumin analogs as potent Nrf2 activators in human bronchial epithelial cells. *Eur. J. Pharm. Sci. 43*, 16-24.

(16) Kumar, V., Kumar, S., Hassan, M., Wu, H., Thimmulappa, R. K., Kumar, A., Sharma, S. K., Parmar, V. S., Biswal, S., and Malhotra, S. V. (2011) Novel chalcone derivatives as potent Nrf2 activators in mice and human lung epithelial cells. *J. Med. Chem. 54*, 4147-4159.

(17) Kobayashi, M., Itoh, K., Suzuki, T., Osanai, H., Nishikawa, K., Katoh, Y., Takagi, Y., and Yamamoto, M. (2002) Identification of the interactive interface and phylogenic conservation of the Nrf2-Keap1 system. *Genes Cells 7*, 807-820.

(18) Li, L., Kobayashi, M., Kaneko, H., Nakajima-Takagi, Y., Nakayama, Y., and Yamamoto, M. (2008) Molecular evolution of Keap1. Two Keap1 molecules with distinctive intervening region structures are conserved among fish. *J. Biol. Chem. 283*, 3248-3255.

(19) Takagi, Y., Kobayashi, M., Li, L., Suzuki, T., Nishikawa, K., and Yamamoto, M. (2004) MafT, a new member of the small Maf protein family in zebrafish. *Biochem. Biophys. Res. Commun. 320*, 62-69.

(20) Itoh, K., Igarashi, K., Hayashi, N., Nishizawa, M., and Yamamoto, M. (1995) Cloning and characterization of a novel erythroid cell-derived CNC family transcription factor heterodimerizing with the small Maf family proteins. *Mol. Cell. Biol. 15*, 4184-4193.

(21) Xi, M. Y., Jia, J. M., Sun, H. P., Sun, Z. Y., Jiang, J. W., Wang, Y. J., Zhang, M. Y., Zhu, J. F., Xu, L. L., Jiang, Z. Y., Xue, X., Ye, M., Yang, X., Gao, Y., Tao, L., Guo, X. K., Xu, X. L., Guo, Q. L., Zhang, X. J., Hu, R., and You, Q. D. (2013) 3-aroylmethylene-2,3,6,7-tetrahydro-1H-pyrazino[2,1-a]isoquinolin-4(11bH)-ones as potent Nrf2/ARE inducers in human cancer cells and AOM-DSS treated mice. *J. Med. Chem. 56*, 7925-7938.

(22) Henderson, C. J., Smith, A. G., Ure, J., Brown, K., Bacon, E. J., and Wolf, C. R. (1998) Increased skin tumorigenesis in mice lacking pi class glutathione S-transferases. *Proc. Natl. Acad. Sci. U. S. A. 95*, 5275-5280.

(23) Harries, L. W., Stubbins, M. J., Forman, D., Howard, G. C., and Wolf, C. R. (1997) Identification of genetic polymorphisms at the glutathione S-transferase Pi

locus and association with susceptibility to bladder, testicular and prostate cancer. *Carcinogenesis 18*, 641-644.

(24) Suzuki, T., Takagi, Y., Osanai, H., Li, L., Takeuchi, M., Katoh, Y., Kobayashi, M., and Yamamoto, M. (2005) Pi class glutathione S-transferase genes are regulated by Nrf 2 through an evolutionarily conserved regulatory element in zebrafish. *Biochem. J. 388*, 65-73.

(25) Tsujita, T., Li, L., Nakajima, H., Iwamoto, N., Nakajima-Takagi, Y., Ohashi, K., Kawakami, K., Kumagai, Y., Freeman, B. A., Yamamoto, M., and Kobayashi, M. (2011) Nitro-fatty acids and cyclopentenone prostaglandins share strategies to activate the Keap1-Nrf2 system: a study using green fluorescent protein transgenic zebrafish. *Genes Cells 16*, 46-57.

(26) Chen, H., Fu, J., Chen, H., Hu, Y., Soroka, D. N., Prigge, J. R., Schmidt, E. E., Yan, F., Major, M. B., Chen, X., and Sang, S. (2014) Ginger compound [6]-shogaol and its cysteine-conjugated metabolite (M2) activate Nrf2 in colon epithelial cells in vitro and in vivo. *Chemical research in toxicology 27*, 1575-1585.

(27) Chen, H., Fu, J., Hu, Y., Soroka, D. N., Prigge, J. R., Schmidt, E. E., Yan, F., Major, M. B., Chen, X., and Sang, S. (2014) Ginger compound [6]-shogaol and its cysteine-conjugated metabolite (M2) activate Nrf2 in colon epithelial cells in vitro and in vivo. *Chem. Res. Toxicol. 27*, 1575-1585.

(28) Zhang, D. D., and Hannink, M. (2003) Distinct cysteine residues in Keap1 are required for Keap1-dependent ubiquitination of Nrf2 and for stabilization of Nrf2 by chemopreventive agents and oxidative stress. *Mol. Cell. Biol. 23*, 8137-8151.

(29) Sang, S., Hong, J., Wu, H., Liu, J., Yang, C. S., Pan, M. H., Badmaev, V., and Ho, C. T. (2009) Increased growth inhibitory effects on human cancer cells and anti-inflammatory potency of shogaols from Zingiber officinale relative to gingerols. *J. Agric. Food Chem. 57*, 10645-10650.

(30) Zhu, Y., Warin, R. F., Soroka, D. N., Chen, H., and Sang, S. (2013) Metabolites of ginger component [6]-shogaol remain bioactive in cancer cells and have low toxicity in normal cells: chemical synthesis and biological evaluation. *PLoS One 8*, e54677.

(31) Tsuge, O., Kanemasa, S., Nakagawa, N., and Suga, H. (1987) Horner-Emmons olefination of 4-hydroxy-2-oxoalkylphosphonates and related compounds: applications to the synthesis of (±)-gingerol, (±)-yashabushiketol, and (±)-dihydroyashabushiketol. *Bull. Chem. Soc. Jpn. 60*, 4091-4098.

(32) Sieber, J. D., Liu, S., and Morken, J. P. (2007) Catalytic conjugate addition of allyl groups to styryl-activated enones. *J. Am. Chem. Soc. 129*, 2214-2215.

(33) Sieber, J. D., and Morken, J. P. (2008) Asymmetric Ni-catalyzed conjugate allylation of activated enones. *J. Am. Chem. Soc. 130*, 4978-4983.

(34) Backstrom, R., Honkanen, E., Pippuri, A., Kairisalo, P., Pystynen, J., Heinola, K., Nissinen, E., Linden, I. B., Mannisto, P. T., Kaakkola, S., and et al. (1989) Synthesis of some novel potent and selective catechol O-methyltransferase inhibitors. *J. Med. Chem. 32*, 841-846.

(35) De Lucia, M., Panzella, L., Pezzella, A., Napolitano, A., and d'Ischia, M. (2008) Plant catechols and their S-glutathionyl conjugates as antinitrosating agents: expedient synthesis and remarkable potency of 5-S-glutathionylpiceatannol. *Chem. Res. Toxicol. 21*, 2407-2413.

(36) Lambert, J. D., Sang, S., Hong, J., Kwon, S. J., Lee, M. J., Ho, C. T., and Yang, C. S. (2006) Peracetylation as a means of enhancing in vitro bioactivity and bioavailability of epigallocatechin-3-gallate. *Drug Metab. Dispos. 34*, 2111-2116.

(37) Shinkai, Y., Sumi, D., Fukami, I., Ishii, T., and Kumagai, Y. (2006) Sulforaphane, an activator of Nrf2, suppresses cellular accumulation of arsenic and its cytotoxicity in primary mouse hepatocytes. *FEBS Lett. 580*, 1771-1774.

(38) Hong, F., Freeman, M. L., and Liebler, D. C. (2005) Identification of sensor cysteines in human Keap1 modified by the cancer chemopreventive agent sulforaphane. *Chem. Res. Toxicol. 18*, 1917-1926.

(39) Maydt, D., De Spirt, S., Muschelknautz, C., Stahl, W., and Muller, T. J. (2013) Chemical reactivity and biological activity of chalcones and other alpha,beta-unsaturated carbonyl compounds. *Xenobiotica 43*, 711-718.

(40) Chen, H., Lv, L., Soroka, D., Warin, R. F., Parks, T. A., Hu, Y., Zhu, Y., Chen, X., and Sang, S. (2012) Metabolism of [6]-shogaol in mice and in cancer cells. *Drug Metab. Dispos. 40*, 742-753.

(41) Luo, Y., Eggler, A. L., Liu, D., Liu, G., Mesecar, A. D., and van Breemen, R. B. (2007) Sites of alkylation of human Keap1 by natural chemoprevention agents. *J. Am. Soc. Mass Spectrom. 18*, 2226-2232.

TOC GRAPHIC

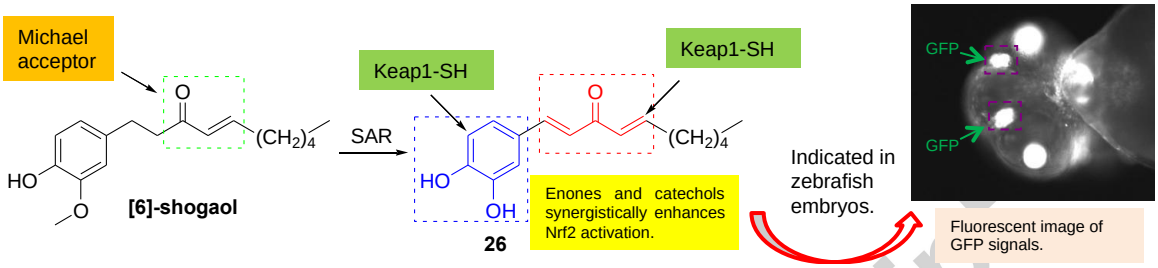

Highlights

- Development of [6]-shogaol (6S) derivatives as potent Nrf2 activators in zebrafish.
- Potency of 6S derivatives relies on *α,β*-unsaturated carbonyl and catechol entities.
- Unsaturated carbonyls and catechols are reactive sites for cysteine conjugation.
- Finding of 6S-derived Nrf2 activators leads to design options for optimization.